Scattering of time-harmonic elastic waves by an elastic inclusion with quadratic nonlinearity

Guangxin Tang
Department of Mechanical Engineering, Northwestern University, 2145 Sheridan Road, Evanston, Illinois 60208

Laurence J. Jacobs
G. W. Woodruff School of Mechanical Engineering, Georgia Institute of Technology, 801 Ferst Drive, Atlanta, Georgia 30332-0405

Jianmin Qu[a)]
Department of Mechanical Engineering, Department of Civil and Environmental Engineering, Northwestern University, 2145 Sheridan Road, Evanston, Illinois 60208

(Received 27 June 2011; revised 8 November 2011; accepted 10 February 2012)

This paper considers the scattering of a plane, time-harmonic wave by an inclusion with heterogeneous nonlinear elastic properties embedded in an otherwise homogeneous linear elastic solid. When the inclusion and the surrounding matrix are both isotropic, the scattered second harmonic fields are obtained in terms of the Green's function of the surrounding medium. It is found that the second harmonic fields depend on two independent acoustic nonlinearity parameters related to the third order elastic constants. Solutions are also obtained when these two acoustic nonlinearity parameters are given as spatially random functions. An inverse procedure is developed to obtain the statistics of these two random functions from the measured forward and backscattered second harmonic fields. [http://dx.doi.org/10.1121/1.3692233]

PACS number(s): 43.25.Ba, 43.25.Dc, 43.20.El [KML] Pages: 2570–2578

I. INTRODUCTION

As a monochromatic ultrasonic wave propagates through a nonlinear elastic solid, higher order harmonics are generated by the material nonlinearity. This phenomena has been observed experimentally in solids since the early 1960s (Breazeale and Thompson, 1963; Cantrell *et al*., 1987), and analytical solutions have been reported in several studies (Lamb, 1925; Keck and Beyer, 1960; Jones and Korbett, 1963; Hikata *et al*., 1965; Thurston and Shapiro, 1967; Zverev and Kalachev, 1968; Thompson *et al*., 1976; Thompson and Tiersten, 1977; Sokolov and Sutin, 1983; Cantrell, 1984; Donskoi and Sutin, 1984; Nazarov *et al*., 1988; Zhou and Shui, 1992; Ostrovsky *et al*., 2003). A rather comprehensive review of the literature in this subject is given by Cantrell (Cantrell, 2004a).

One of the recent applications of second harmonic generation is nondestructive evaluation of fatigue damage in polycrystalline solids (Herrmann *et al*., 2006; Kim *et al*., 2006a; Kim *et al*., 2006b; Bermes *et al*., 2007; Pruell *et al*., 2007; Bermes *et al*., 2008). Under cyclic loading, dislocation are generated and multiplied. It is postulated that these dislocations give rise to material nonlinearity that generates the second harmonics in the propagating ultrasonic wave (Suzuki *et al*., 1964; Hikata *et al*., 1965; Hikata and Elbaum, 1966). Because monitoring individual dislocation is extremely difficult due to their small size and large quantity, fatigue damage is usually characterized by plastic deformation in polycrystalline solids. Since plastic strain, in essence, is a collective manifestation of numerous dislocations, the magnitude of the second harmonics can be related to the dislocation density via the plastic strain (Kim *et al*., 2006b). In most ultrasonic tests, the measurable parameter that characterizes the dislocation density or plastic strain is the ultrasonic nonlinearity parameter β. Numerous experimental data have demonstrated the correlation between the magnitude of β and the degree of fatigue induced damage, e.g., Herrmann *et al*. (2006); Kim *et al*. (2006a); Kim *et al*. (2006b); Bermes *et al*. (2007); Pruell *et al*. (2007); Bermes *et al*. (2008).

A polycrystalline solid is an assembly of numerous single crystals (grains) with different orientations. When subjected to cyclic loading, certain grains will become plastically deformed because of their preferentially oriented slip planes. As the number of loading cycles increases, more and more grains will become plastically deformed. Eventually, plastic deformation may occur uniformly in all grains and the material fails by gross plasticity. A more likely scenario, however, is that grains near certain regions will become more and more plastically deformed to form localized damage zones such as slip bands and microcracks. The nature of such localized failure is dictated by the particular distribution of the plastic strain field, which, among other things, depends on the stress distribution, the microstructure of the polycrystalline assembly, and the initial distribution of defects. Recent advances in fatigue analysis have shown the potential to estimate the remaining fatigue life based on the plastic strain distributions. It would thus be extremely useful to develop nondestructive techniques to evaluate the plastic

[a)]Author to whom correspondence should be addressed. Electronic mail: j-qu@northwestern.edu

 0001-4966/2012/131(4)/2570/9/$30.00

strain distribution in structural components subjected to cyclic loading. Since the acoustic nonlinearity parameter β is intimately related to the plastic strain (Kim *et al.*, 2006b), measurements of the spatial distribution of β can provide information on the distribution of plastic strain.

Most of the existing studies in the literature, either experimental, numerical, or analytical, have assumed that the nonlinear parameter β is a constant over the entire path of the wave propagation. Since β is directly related to the plastic strain field, such an assumption implies that the plastic strain field developed under cyclic loading is also uniform. To account for the non-uniformity or heterogeneity in the plastic strain fields, solutions are needed for the wave equation when β is spatially dependent.

In this paper, we consider the case of a plane time-harmonic wave propagating in a three-dimensional medium with heterogeneous quadratic nonlinearity, i.e., the acoustic nonlinearity parameter(s) are not spatially uniform. To simplify the algebra, we assume that the linear properties of the medium such as the mass density and second order elastic constants are uniform. This assumption is reasonable when the medium is a polycrystalline solid, because, in this case, all the grains are made of the same crystal. They are simply oriented differently in the polycrystalline assembly. Therefore, the mass density of each grain is the same. The second order elastic constants, although anisotropic, differ among the grains only by a coordinate rotation. When the wavelength is much greater than the grain size, the polycrystalline solid can be viewed as an isotropic and homogeneous solid for linear elastic waves. Heterogeneity of the acoustic nonlinearity parameters only affects the second harmonic of the wave fields.

We note that non-uniform β in liquids have been treated extensively in the literature, e.g., Donskoi and Sutin (1980); Sokolov and Sutin (1983); Donskoi and Sutin (1984); Nazarov *et al.* (1988). Obviously, the major distinction between solids and fluids is the complexity arising from the shear wave and its interactions with the longitudinal waves in solids. As shown in this paper, two independent acoustic nonlinearity parameters are needed to describe the second harmonic in an isotropic solid.

II. GOVERNING EQUATIONS IN NONLINEAR MEDIA

To describe the wave motion, a Cartesian coordinate system $x_i (i = 1, 2, 3)$ is affixed to the continuum elastic body of interest, where the coordinate x_i is also used to label the material particle that was located at x_i in the initial (undeformed) configuration. This way of describing the wave motion is called the Lagrangian description and x_i is called the Lagrangian coordinate. At any given time t, the displacement of the particle x_i from its initial location is denoted by $u_i = u_i(\mathbf{x}, t)$. The displacement equations of motion is given by (Norris, 1997)

$$\rho_0 \frac{\partial^2 u_i}{\partial t^2} - \frac{\partial}{\partial x_j}\left(C_{ijkl}\frac{\partial u_k}{\partial x_l}\right) = L_{ijklmn}\frac{\partial u_m}{\partial x_n}\frac{\partial^2 u_k}{\partial x_j \partial x_l} + \frac{1}{2}\frac{\partial L_{ijklmn}}{\partial x_j}\frac{\partial u_k}{\partial x_l}\frac{\partial u_m}{\partial x_n}, \quad (1)$$

where ρ_0 is the mass density of the undeformed solid, C_{ijkl} is the second order elastic stiffness tensor, and L_{ijklmn} is a linear combination of C_{ijkl} and the third order elastic stiffness C_{ijklmn}. For isotropic solids,

$$C_{ijkl} = \lambda\delta_{ij}\delta_{kl} + 2\mu I_{ijkl}, \quad (2)$$

$$C_{ijklmn} = (2l - 2m + n)\delta_{ij}\delta_{kl}\delta_{mn} + (2m - n) \times (\delta_{ij}I_{klmn} + \delta_{kl}I_{mnij} + \delta_{mn}I_{ijkl}) + \frac{n}{2}(\delta_{ik}I_{jlmn} + \delta_{il}I_{jkmn} + \delta_{jk}I_{ilmn} + \delta_{jl}I_{ikmn}), \quad (3)$$

$$L_{ijklmn} = C_{ijklmn} + \lambda(\delta_{ij}\delta_{ln}\delta_{km} + \delta_{jl}\delta_{mn}\delta_{ik} + \delta_{jn}\delta_{kl}\delta_{im}) + 2\mu(I_{ijln}\delta_{km} + I_{jlmn}\delta_{ik} + I_{jnkl}\delta_{im}), \quad (4)$$

where λ and μ are the Lamé constants, l, m, and n are the Murnaghan third order elastic (TOE) constants, δ_{ij} is the Kronecker delta, and $I_{ijkl} = (\delta_{ik}\delta_{jl} + \delta_{il}\delta_{jk})/2$ is the fourth order identity tensor.

Furthermore, we assume that the Lamé constants are spatially homogeneous (independent of spatial coordinates), while the TOE is spatially inhomogeneous. Thus, making use of Eqs. (2)–(4) in Eq. (1) leads to the equations of motion for isotropic material

$$\frac{1}{c_L^2}\frac{\partial^2 u_i}{\partial t^2} - \left(1 - \frac{1}{\kappa^2}\right)\frac{\partial^2 u_j}{\partial x_j \partial x_i} - \frac{1}{\kappa^2}\frac{\partial^2 u_i}{\partial x_j \partial x_j} = f_i, \quad (5)$$

where $\kappa = c_L/c_T$, $c_L = \sqrt{(\lambda + 2\mu)/\rho_0}$, $c_T = c_S = \sqrt{\mu/\rho_0}$, and

$$f_i = \frac{1}{\lambda + 2\mu}\left[L_{ijklmn}\frac{\partial u_m}{\partial x_n}\frac{\partial^2 u_k}{\partial x_j \partial x_l} + \frac{1}{2}\frac{\partial C_{ijklmn}}{\partial x_j}\frac{\partial u_k}{\partial x_l}\frac{\partial u_m}{\partial x_n}\right]. \quad (6)$$

Equations (5) and (6) are the equations governing wave motions in a hyperelastic material with quadratic nonlinearity. Using the vector notation, Eq. (5) can be written symbolically as

$$L[\mathbf{u}] = \mathbf{f}[\mathbf{u}], \quad (7)$$

where the differential operator is linear and given by

$$L[\mathbf{u}] = \frac{1}{c_L^2}\frac{\partial^2 \mathbf{u}}{\partial t^2} - \left(1 - \frac{1}{\kappa^2}\right)\nabla(\nabla \cdot \mathbf{u}) - \frac{1}{\kappa^2}\nabla^2 \mathbf{u}, \quad (8)$$

and the function $\mathbf{f}[\mathbf{u}]$ contains all the nonlinear terms given in Eq. (6).

III. SCATTERED FIELDS

Consider a homogeneous elastic solid of infinite extent. Let a large plastic strain field be distributed over a finite domain V inside this homogeneous elastic solid. As discussed below, due to the large plastic strain field, the acoustic nonlinearity in V is much larger than that in the surrounding matrix, so that the latter can be assumed to be zero. Such a domain V is called an inclusion in the literature (Qu and Cherkaoui, 2006).

Without loss of generality, let the incident wave be a time-harmonic plane wave

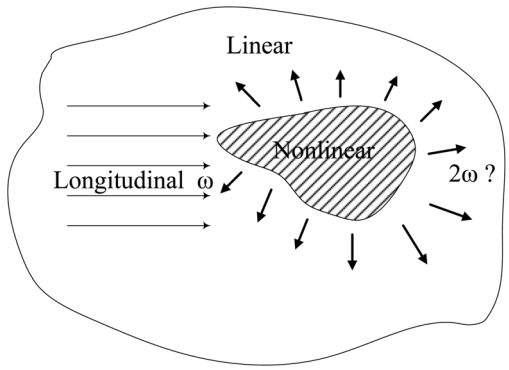

FIG. 1. An incident longitudinal wave with circular frequency ω impinges upon a nonlinear inclusion embedded in a linear medium. Since the linear properties of the medium are uniform, the scattered field will not contain the fundamental frequency. Only second harmonic 2ω will be scattered.

$$u_i^{(1)} = \delta_{i1} U \cos(\omega t - k_L x_1), \tag{9}$$

where $k_L = \omega/c_L$ is the longitudinal wavenumber in the elastic solids. For future reference, $k_T = \omega/c_T = k_S$ is reserved for the transverse wavenumber. Since the inclusion and the surrounding medium have identical second order elastic properties, the scattered field will not contain the fundamental frequency (Fig. 1). Only higher order waves are generated by the nonlinearity of the inclusion. In this paper, we are only interested in the second order waves in the scattered field $u_i^{(2)}$, so that the total wave field (incident plus the scattered) is given by

$$\mathbf{u} = \mathbf{u}^{(1)} + \mathbf{u}^{(2)}. \tag{10}$$

Since the nonlinearity is weak, it may be assumed that $|\mathbf{u}^{(2)}| \ll |\mathbf{u}^{(1)}|$. Consequently, following a standard perturbation procedure by keeping terms up to the second harmonic, one may rewrite the equations of motion (7) as

$$L\,[\mathbf{u}^{(2)}] = \begin{cases} 0 & \mathbf{x} \notin V \\ \mathbf{f}[\mathbf{u}^{(1)}] & \mathbf{x} \in V, \end{cases} \tag{11}$$

where

$$\mathbf{f}[\mathbf{u}^{(1)}] = \mathbf{s}(\mathbf{x}) + \mathrm{Re}\{\mathbf{h}(\mathbf{x}) \exp(-2i\omega t)\}. \tag{12}$$

The notation $\mathrm{Re}\{*\}$ means the real part of $\{*\}$, and

$$s_j(\mathbf{x}) = -\frac{U^2\omega^2}{4c_L^2}\left[\frac{\partial \beta_L}{\partial x_j} - \frac{\partial \beta_S}{\partial x_j} + \frac{\partial \beta_S}{\partial x_1}\delta_{j1}\right], \tag{13}$$

$$h_j(\mathbf{x}) = \frac{U^2\omega^2}{4c_L^2}\exp(2ik_L x_1) \times \left[\frac{\partial \beta_L}{\partial x_j} - \frac{\partial \beta_S}{\partial x_j} + \left(2ik_L\beta_L + \frac{\partial \beta_S}{\partial x_1}\right)\delta_{j1}\right], \tag{14}$$

with

$$\beta_L = -\left(3 + \frac{4m+2l}{\lambda+2\mu}\right), \quad \beta_S = -2\left(\frac{\lambda+3\mu}{\lambda+2\mu} + \frac{2m}{\lambda+2\mu}\right), \tag{15}$$

where β_L and β_S are the acoustic nonlinearity parameters related to both geometrical and elastic nonlinearity. Typical values of the acoustic nonlinearity parameters are $6 < \beta_L < 11$, $4 < \beta_S < 8$ for steels, and $8 < \beta_L < 24$, $5 < \beta_S < 17$ for aluminum alloys (Smith *et al.*, 1966).

We note that β_L and β_S defined above are independent of each other in that they depend on different TOE constants. The β_L given in Eq. (15) is the same as the acoustic nonlinearity parameter associated with a one-dimensional longitudinal wave. The β_S given in Eq. (15), however, is not the same as the acoustic nonlinearity parameter $\beta_T = (\lambda + 2\mu + m)/\mu$. This β_T is associated with the interaction between a longitudinal wave and a transverse wave when they are propagating in the same direction. The β_S given in Eq. (15), however, is associated with the second harmonic shear wave induced by the mode conversion (from the fundamental longitudinal to shear) at an interface (Zhou and Shui, 1992).

Another important consideration is that, for simplicity, only the geometrical and elastic nonlinearities are included in Eq. (15). For example, in β_L, the term -3 is from the geometrical nonlinearity, and the term $-(4m+2l)/(\lambda+2\mu)$ is from the elastic nonlinearity. In addition to the geometrical and elastic nonlinearities, it has been shown, e.g., Cantrell (2004b); Kim *et al.* (2006b), that plastic deformation (which is a consequence of dislocation dynamics) also contributes to β_L. For most metallic materials, geometrical and elastic nonlinearities do not change with fatigue damage, while plastic strains accumulate with increasing fatigue cycles. Extensive experimental data (Herrmann *et al.*, 2006; Kim *et al.*, 2006a; Kim *et al.*, 2006b; Bermes *et al.*, 2007; Pruell *et al.*, 2007; Bermes *et al.*, 2008) have shown that plastic deformation induced acoustic nonlinearity due to fatigue damage is often much larger than geometrical and elastic nonlinearities. This justifies the earlier assumption that, in comparison with the large acoustic nonlinearity in V due to fatigue damage, the acoustic nonlinearity in the matrix is negligible.

In the rest of this paper, β_L and β_S will be used symbolically to represent the acoustic nonlinearity in V, so that all the results are valid irrespective of the specific expressions of β_L and β_S such as those given in Eq. (15). Therefore, conclusions obtained in this paper are also valid when the contributions to β_L and β_S due to fatigue damage are considered.

Clearly, $s_j(\mathbf{x})$ represents a static body force and $h_j(\mathbf{x})$ is a harmonic body force in Eq. (11). Since the differential operator $L\,[\mathbf{u}^{(2)}]$ is linear, the solution to Eq. (11) is a superposition of the solutions corresponding to $s_j(\mathbf{x})$ and $h_j(\mathbf{x})$, respectively.

Let us first consider the solution corresponding to $h_j(\mathbf{x})$. The linearity of Eq. (11) allows us to drop the time-harmonic factor $\exp(-2i\omega t)$ so the solution can be written as

$$u_j^h(\mathbf{x}) = \int_{V^+} G_{jk}(\mathbf{x}, \mathbf{y}) h_k(\mathbf{y}) d\mathbf{y}, \quad \text{for } \mathbf{x} \notin V, \tag{16}$$

where $G_{jk}(\mathbf{x}, \mathbf{y})$ is the steady state Green's function of Eq. (11),

$$G_{jk}(\mathbf{x}, \mathbf{y}) = \frac{\kappa^2}{4\pi}\left[\frac{e^{2ik_T r}}{r}\delta_{jk} + \frac{c_T^2}{(2\omega)^2}\frac{\partial^2}{\partial x_j \partial x_k}\left(\frac{e^{2ik_T r}}{r} - \frac{e^{2ik_L r}}{r}\right)\right], \quad r = \|\mathbf{x} - \mathbf{y}\|. \tag{17}$$

The notation V^+ is to emphasize that the integral is over the closed region occupied by V. Since $\beta_L = \beta_S = 0$ is outside of V, one may substitute Eq. (14) into Eq. (16) and carry out integration by parts to remove the derivatives on β_L and β_S,

$$u_j^h(\mathbf{x}) = -\frac{U^2\omega^2}{4c_L^2}\int_V [\beta_L(\mathbf{y}) - \beta_S(\mathbf{y})]\frac{\partial G_{jk}(\mathbf{x},\mathbf{y})}{\partial y_k}\exp(2ik_L y_1)d\mathbf{y} - \frac{U^2\omega^2}{4c_L^2}\int_V \beta_S(\mathbf{y})\frac{\partial G_{j1}(\mathbf{x},\mathbf{y})}{\partial y_1}\exp(2ik_L y_1)d\mathbf{y}. \quad (18)$$

Note that the first term on the right-hand side of Eq. (18) is purely irrotational, representing a dilatational longitudinal wave radiating from the inclusion. In other words, when $\beta_S(\mathbf{y}) = 0$, the scattered second harmonic wave is a longitudinal wave.

In a similar manner, the static solution corresponding to $\mathbf{s}$ can be written as

$$u_j^s(\mathbf{x}) = \int_{V^+} \hat{G}_{jk}(\mathbf{x},\mathbf{y})s_k(\mathbf{y})d\mathbf{y}, \quad \text{for} \quad \mathbf{x} \notin V, \quad (19)$$

where the static Green's function is given by

$$\hat{G}_{jk}(\mathbf{x},\mathbf{y}) = \lim_{\omega\to 0} G_{jk}(\mathbf{x},\mathbf{y}) = \frac{\kappa^2}{8\pi r}\left[\left(1+\frac{1}{\kappa^2}\right)\delta_{jk} + \left(1-\frac{1}{\kappa^2}\right)\times\frac{(x_j-y_j)(x_k-y_k)}{r^2}\right]. \quad (20)$$

Removing the derivatives on β_L and β_S in Eq. (19) leads to

$$u_j^s(\mathbf{x}) = \frac{U^2\omega^2}{4c_L^2}\int_V [\beta_L(\mathbf{y}) - \beta_S(\mathbf{y})]\frac{\partial \hat{G}_{jk}(\mathbf{x},\mathbf{y})}{\partial y_k}d\mathbf{y} + \frac{U^2\omega^2}{4c_L^2}\int_V \beta_S(\mathbf{y})\frac{\partial \hat{G}_{j1}(\mathbf{x},\mathbf{y})}{\partial y_1}d\mathbf{y}. \quad (21)$$

This static displacement gives rise to the radiation-induced eigenstrain (Qu *et al.*, 2011). Since the integrands decay with r^{-2} in the far field, one can conclude that the static displacement vanishes far away from the inclusion.

Finally, the total scattered field is given by

$$u_j^{(2)}(\mathbf{x},t) = u_j^s(\mathbf{x}) + \mathrm{Re}\{u_j^h(\mathbf{x})\exp(-2i\omega t)\}, \quad \text{for} \quad \mathbf{x}\notin V. \quad (22)$$

IV. FAR-FIELD APPROXIMATIONS

For many applications in nondestructive evaluation, it is useful to derive the far-field approximations under the condition $(\omega/c_L)\|\mathbf{x}-\mathbf{y}\| \gg 1$ for $\mathbf{y}\in V$. In this case, the Green's function is approximately given by (Achenbach *et al.*, 1982)

$$G_{jk} \approx G_{jk}^L + G_{jk}^S, \quad (23)$$

where

$$G_{jk}^\alpha = g_{jk}^\alpha(\hat{\mathbf{x}})\frac{\exp(2ik_\alpha\|\mathbf{x}\|)}{4\pi\|\mathbf{x}\|}\exp(-2ik_\alpha\mathbf{y}\cdot\hat{\mathbf{x}}), \quad \hat{\mathbf{x}} = \frac{\mathbf{x}}{\|\mathbf{x}\|}, \quad \alpha = L,S, \quad (24)$$

$$g_{jk}^L(\hat{\mathbf{x}}) = \hat{x}_j\hat{x}_k, \quad g_{jk}^S(\hat{\mathbf{x}}) = \kappa^2(\delta_{jk} - \hat{x}_j\hat{x}_k). \quad (25)$$

It can be shown that G_{jk}^L and G_{jk}^S in Eq. (23) represent a longitudinal and a transverse wave, respectively, with propagation direction defined by $\hat{x}_i$.

Substituting Eqs. (23)–(25) into Eq. (16) yields

$$u_j^h = \frac{A_j^L(\hat{\mathbf{x}})\exp(2ik_L\|\mathbf{x}\|)}{4\pi\|\mathbf{x}\|} + \frac{A_j^S(\hat{\mathbf{x}})\exp(2ik_T\|\mathbf{x}\|)}{4\pi\|\mathbf{x}\|}, \quad (26)$$

where

$$A_j^\alpha(\hat{\mathbf{x}}) = g_{jk}^\alpha(\hat{\mathbf{x}})\int_{V^+}\exp(-2ik_\alpha\mathbf{y}\cdot\hat{\mathbf{x}})h_k(\mathbf{y})d\mathbf{y}, \quad \alpha = L\,,\ S. \quad (27)$$

Clearly, Eq. (26) represents two spherical waves, one is a longitudinal wave with amplitude A_j^L and the other is a shear wave with amplitude A_j^S. Similar to deriving Eq. (18), the derivatives on β_L and β_S in Eq. (27) can be removed by carrying out integration by parts. Thus, making use of Eq. (25) leads to

$$A_j^L(\hat{\mathbf{x}}) = \frac{iU^2k_L^3}{2}[\phi_L(\hat{\mathbf{x}}) - (1-\hat{x}_1^2)\psi_L(\hat{\mathbf{x}})]\hat{x}_j, \quad (28)$$

$$A_j^S(\hat{\mathbf{x}}) = \frac{iU^2k_T^3}{2}(\delta_{j1} - \hat{x}_j\hat{x}_1)\hat{x}_1\psi_S(\hat{\mathbf{x}}), \quad (29)$$

where

$$\phi_\alpha(\hat{\mathbf{x}}) = \int_V \beta_L(\mathbf{y})\exp(-2ik_\alpha\mathbf{y}\cdot\hat{\mathbf{x}} + 2ik_Ly_1)d\mathbf{y}, \quad (30)$$

$$\psi_\alpha(\hat{\mathbf{x}}) = \int_V \beta_S(\mathbf{y})\exp(-2ik_\alpha\mathbf{y}\cdot\hat{\mathbf{x}} + 2ik_Ly_1)d\mathbf{y}, \quad (31)$$

Again, if $\beta_S(\mathbf{y}) = 0$, then $\psi_\alpha(\hat{\mathbf{x}}) = 0$. Consequently, Eq. (29) is equal to zero, i.e., there is no shear wave.

It follows from Eqs. (28) and (29) that the magnitude of these spherical waves can be written as

$$A^L(\hat{\mathbf{x}}) \equiv \sqrt{A_j^L(\hat{\mathbf{x}})A_j^{L*}(\hat{\mathbf{x}})} = \frac{U^2k_L^3}{2}\sqrt{|\phi_L(\hat{\mathbf{x}})|^2 - 2(1-\hat{x}_1^2)\mathrm{Re}\{\psi_L^*(\hat{\mathbf{x}})\phi_L(\hat{\mathbf{x}})\} + (1-\hat{x}_1^2)^2|\psi_L(\hat{\mathbf{x}})|^2}, \quad (32)$$

$$A^S(\hat{\mathbf{x}}) \equiv \sqrt{A_j^S(\hat{\mathbf{x}})A_j^{S*}(\hat{\mathbf{x}})}$$
$$= \frac{U^2 k_T^3}{2}\sqrt{(1-\hat{x}_1^2)}|\hat{x}_1\psi_S(\hat{\mathbf{x}})|. \quad (33)$$

As an example, we chose $\beta_S = 0.7\beta_L =$ constant in Eqs. (28)–(31), and V as a sphere with radius R. The directional dependences of Eqs. (32) and (33) in the plane crossing the center of the sphere V normalized by $U^2k_L^3V\beta_L/2$ are plotted in Figs. 2(a) and 2(b), respectively. It is seen from Fig. 2(a) that at very low frequencies ($k_LR = 0.01$) the spherical inclusion acts like a dipole that scatters the second harmonic longitudinal wave mainly in the forward and backward directions. As the frequency increases, the backscattered second harmonic longitudinal wave starts to diminish. In the intermediate frequency regime ($k_LR = 1$), only the forward lobe remains. In the high frequency regime ($k_LR = 100$), the forward lobe reduces to needle shape in the forward direction, e.g., all the scattered second harmonic field is limited to the forward direction only. The situation is somewhat different for the scattered second harmonic shear wave, see Fig. 2(b). In the low frequency regime, the inclusion acts like a quadruple generating scattered second harmonic shear waves in four perpendicular directions with almost identical amplitude. As the frequency increases, amplitude of the scattered second harmonic shear wave starts to diminish in all directions with a much faster rate in the backward direction. In the intermediate frequency regime, only the lobes in the forward direction remain. In the high frequency regime, the scattered second harmonic shear wave almost disappears in the far field.

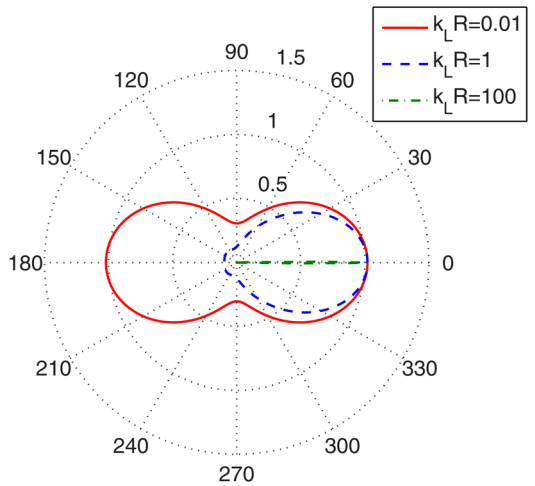

(a)

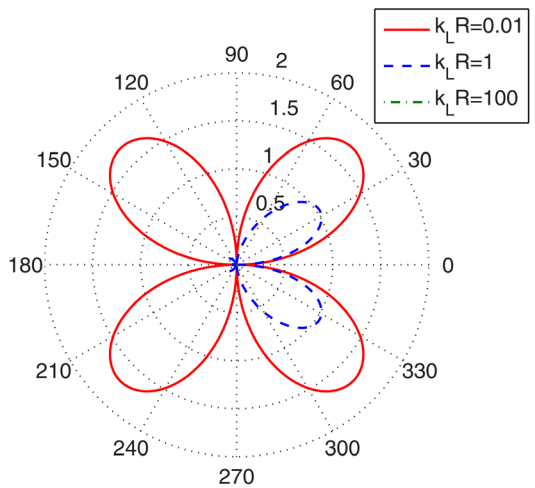

(b)

FIG. 2. (Color online) (a) Normalized amplitude directivity of the second harmonic longitudinal wave in far-field scattered by a spherical nonlinear inclusion with radius R. $k_L = \omega/c_L$ is the wave number of the incident longitudinal wave, which propagates in the direction of 0°. (b) Normalized amplitude directivity of the second harmonic shear wave in far-field scattered by a spherical nonlinear inclusion with radius R. $k_L = \omega/c_L$ is the wave number of the incident longitudinal wave, which propagates in the direction of 0°.

Similarly, the far-field approximation of the static Green's function (20) is given by

$$\hat{G}_{ij}(\mathbf{x},\mathbf{y}) = \frac{(\kappa^2+1)\delta_{ij} + (\kappa^2-1)\hat{x}_i\hat{x}_j}{8\pi\|\mathbf{x}\|}. \quad (34)$$

Since $\hat{G}_{ij}(\mathbf{x},\mathbf{y})$ is independent of $\mathbf{y}$, it is clear from Eq. (21) that $u_i^s(\mathbf{x}) = 0$ for $\mathbf{x}$ far away from the inclusion.

Of great interest in practice are the forward scattered and backscattered fields. In the forward direction, $\hat{x}_j = \hat{x}_j^f = \delta_{j1}$. Thus,

$$A_j^L(\hat{\mathbf{x}}^f) = \frac{iU^2k_L^3}{2}\phi_L(\hat{\mathbf{x}}^f)\delta_{j1}, \quad A_j^S(\hat{\mathbf{x}}^f) = 0,$$
$$A^L(\hat{\mathbf{x}}^f) = \frac{U^2k_L^3}{2}\sqrt{\phi_L(\hat{\mathbf{x}}^f)\phi_L^*(\hat{\mathbf{x}}^f)}, \quad (35)$$

where

$$\phi_L(\hat{\mathbf{x}}^f) = \int_V \beta_L(\mathbf{y})d\mathbf{y}. \quad (36)$$

In the backward direction, $\hat{x}_j = \hat{x}_j^b = -\delta_{j1}$. Thus,

$$A_j^L(\hat{\mathbf{x}}^b) = \frac{-iU^2k_L^3}{2}\phi_L(\hat{\mathbf{x}}^b)\delta_{j1}, \quad A_j^S(\hat{\mathbf{x}}^b) = 0,$$
$$A^L(\hat{\mathbf{x}}^f) = \frac{U^2k_L^3}{2}\sqrt{\phi_L(\hat{\mathbf{x}}^b)\phi_L^*(\hat{\mathbf{x}}^b)}, \quad (37)$$

where

$$\phi_L(\hat{\mathbf{x}}^b) = \int_V \beta_L(\mathbf{y})\exp(4ik_Ly_1)d\mathbf{y}. \quad (38)$$

These results will be used in Sec. V to determine the nonlinearity parameters through the forward and backscattered waves.

V. STOCHASTIC NONLINEAR PROPERTIES OF THE INCLUSION

Consider the case when the nonlinear properties of the inclusion $\beta_\alpha(\mathbf{x})$, $\alpha = L, S$, are random functions of $\mathbf{x}$, i.e., they represent random (stochastic) processes. For simplicity, we assume that these random processes are ergodic, i.e., the

ensemble average (mean) $\langle\beta_\alpha(\mathbf{x})\rangle$ is independent of the spatial coordinate $\mathbf{x}$, and is equal to its spatial averages, i.e.,

$$\langle\beta_\alpha\rangle \equiv \int_{-\infty}^{\infty} \xi p_\alpha(\xi)d\xi = \frac{1}{V}\int_V \beta_\alpha(\mathbf{x})d\mathbf{x}, \tag{39}$$

where $p_\alpha(\mathbf{x},\xi) = p_\alpha(\xi)$ is the probability density functions (PDF) of $\beta_\alpha(\mathbf{x})$ at location $\mathbf{x}$. The autocorrelation function of $\beta_\alpha(\mathbf{x})$ is given by

$$\begin{aligned} N_{\alpha\alpha}(\boldsymbol{\tau},\boldsymbol{\upsilon}) &\equiv \langle\beta_\alpha(\boldsymbol{\tau})\beta_\alpha(\boldsymbol{\upsilon})\rangle \\ &= \int_{-\infty}^{\infty}\int_{-\infty}^{\infty} \xi_1\xi_2 p_\alpha(\xi_1,\xi_2;\boldsymbol{\tau},\boldsymbol{\upsilon})d\xi_1 d\xi_2 \\ &= \frac{1}{V^2}\int_V\int_V \beta_\alpha(\mathbf{y}_1;\boldsymbol{\tau})\beta_\alpha(\mathbf{y}_2;\boldsymbol{\upsilon})d\mathbf{y}_1 d\mathbf{y}_2, \end{aligned} \tag{40}$$

where $p_\alpha(\xi_1,\xi_2;\boldsymbol{\tau},\boldsymbol{\upsilon})$ is the second order PDF. The last equality in Eq. (40) is a consequence of the ergodicity of the process. In a similar manner, the cross-correlation function between $\beta_L(\mathbf{x})$ and $\beta_S(\mathbf{x})$ is given by

$$\begin{aligned} N_{LS}(\boldsymbol{\tau},\boldsymbol{\upsilon}) &\equiv \langle\beta_L(\boldsymbol{\tau})\beta_S(\boldsymbol{\upsilon})\rangle \\ &= \int_{-\infty}^{\infty}\int_{-\infty}^{\infty} \xi_1\xi_2 p_{LS}(\xi_1,\xi_2;\boldsymbol{\tau},\boldsymbol{\upsilon})d\xi_1 d\xi_2 \\ &= \frac{1}{V^2}\int_V\int_V \beta_L(\mathbf{y}_1;\boldsymbol{\tau})\beta_S(\mathbf{y}_2;\boldsymbol{\upsilon})d\mathbf{y}_1 d\mathbf{y}_2. \end{aligned} \tag{41}$$

Next, treat A_j^α as random variables of the stochastic processes $\beta_\alpha(\mathbf{x})$. For each particular realization $\beta_\alpha(\mathbf{x})$, the values of A_j^α can be determined from Eqs. (28) and (29). The expected (mean) values or ensemble averages of these random variables can then be written as

$$\langle A_j^L(\hat{\mathbf{x}})\rangle = \frac{iU^2k_L^3}{2}[\langle\phi_L(\hat{\mathbf{x}})\rangle - (1-\hat{x}_1^2)\langle\psi_L(\hat{\mathbf{x}})\rangle]\hat{x}_j, \tag{42}$$

$$\langle A_j^S(\hat{\mathbf{x}})\rangle = \frac{iU^2k_T^3}{2}(\delta_{j1} - \hat{x}_j\hat{x}_1)\hat{x}_1\langle\psi_S(\hat{\mathbf{x}})\rangle, \tag{43}$$

where

$$\langle\phi_\alpha(\hat{\mathbf{x}})\rangle = \langle\beta_L\rangle V_\alpha(\hat{\mathbf{x}}), \quad \langle\psi_\alpha(\hat{\mathbf{x}})\rangle = \langle\beta_S\rangle V_\alpha(\hat{\mathbf{x}}), \tag{44}$$

and

$$V_\alpha(\hat{\mathbf{x}}) = \int_V \exp(-2ik_\alpha\mathbf{y}\cdot\hat{\mathbf{x}} + 2ik_L y_1)d\mathbf{y}, \tag{45}$$

which can be readily evaluated once the geometry of the inclusion is known.

In a similar manner, the ensemble average of the squared amplitude of the scattered fields can also be obtained in terms of the correlations functions,

$$\begin{aligned} \langle A_j^L A_j^{L*}\rangle = \frac{U^4k_L^6}{4}[&\langle\phi_L\phi_L^*\rangle - 2(1-\hat{x}_1^2)\mathrm{Re}\langle\psi_L^*\phi_L\rangle \\ &+(1-\hat{x}_1^2)^2\langle\psi_L\psi_L^*\rangle], \end{aligned} \tag{46}$$

$$\langle A_j^S A_j^{S*}\rangle = \frac{U^4k_T^6}{4}(1-\hat{x}_1^2)\hat{x}_1^2\langle\psi_S\psi_S^*\rangle, \tag{47}$$

where

$$\begin{aligned} \langle\phi_\alpha\phi_\alpha^*\rangle = &\int_V\int_V N_{LL}(\boldsymbol{\tau},\boldsymbol{\upsilon}) \\ &\times\exp[-2ik_\alpha(\boldsymbol{\tau}-\boldsymbol{\upsilon})\cdot\hat{\mathbf{x}} + 2ik_L(\tau_1-\upsilon_1)]d\boldsymbol{\tau}d\boldsymbol{\upsilon}, \end{aligned} \tag{48}$$

$$\begin{aligned} \langle\psi_\alpha\psi_\alpha^*\rangle = &\int_V\int_V N_{SS}(\boldsymbol{\tau},\boldsymbol{\upsilon}) \\ &\times\exp[-2ik_\alpha(\boldsymbol{\tau}-\boldsymbol{\upsilon})\cdot\hat{\mathbf{x}} + 2ik_L(\tau_1-\upsilon_1)]d\boldsymbol{\tau}d\boldsymbol{\upsilon}, \end{aligned} \tag{49}$$

$$\begin{aligned} \langle\phi_\alpha\psi_\alpha^*\rangle = &\int_V\int_V N_{LS}(\boldsymbol{\tau},\boldsymbol{\upsilon}) \\ &\times\exp[-2ik_\alpha(\boldsymbol{\tau}-\boldsymbol{\upsilon})\cdot\hat{\mathbf{x}} + 2ik_L(\tau_1-\upsilon_1)]d\boldsymbol{\tau}d\boldsymbol{\upsilon}. \end{aligned} \tag{50}$$

These expressions can be significantly simplified for the forward and backscattered fields. Specifically, in the forward direction, $\hat{x}_j = \hat{x}_j^f = \delta_{j1}$. Thus, we have $\langle A_j^S\rangle_f = 0$, $\langle A_j^S A_j^{S*}\rangle_f = 0$ and

$$\begin{aligned} \langle A_j^L\rangle_f &= \frac{iU^2k_L^3}{2}\langle\beta_L\rangle V\delta_{j1}, \\ \langle A_j^L A_j^{L*}\rangle_f &= \frac{U^4k_L^6}{4}\langle\phi_L\phi_L^*\rangle_f, \end{aligned} \tag{51}$$

where

$$\langle\phi_L\phi_L^*\rangle_f = \int_V\int_V N_{LL}(\boldsymbol{\tau},\boldsymbol{\upsilon})d\boldsymbol{\tau}d\boldsymbol{\upsilon}. \tag{52}$$

In the backward direction, $\hat{x}_i^b = -\delta_{i1}$. It then follows from Eqs. (43) and (47) that $\langle A_j^S\rangle_b = 0$, $\langle A_j^S A_j^{S*}\rangle_b = 0$, and

$$\begin{aligned} \langle A_j^L\rangle_b &= -\frac{iU^2k_L^3}{2}\langle\beta_L\rangle V_L(\hat{\mathbf{x}}^b)\delta_{j1}, \\ \langle A_j^L A_j^{L*}\rangle_b &= \frac{U^4k_L^6}{4}\langle\phi_L\phi_L^*\rangle_b, \end{aligned} \tag{53}$$

where

$$\begin{aligned} V_L(\hat{\mathbf{x}}^b) &= \int_V \exp(4ik_L y_1)d\mathbf{y}, \\ \langle\phi_L\phi_L^*\rangle_b &= \int_V\int_V N_{LL}(\boldsymbol{\tau},\boldsymbol{\upsilon})\exp[4ik_L(\tau_1-\upsilon_1)]d\boldsymbol{\tau}d\boldsymbol{\upsilon}. \end{aligned} \tag{54}$$

The above equations establish the relationship between the scattered far fields and the stochastic nonlinear properties of the inclusion. Once the statistics of $\beta_\alpha(\mathbf{x})$ is known throughout the inclusion, the statistics of the scattered fields can be evaluated from the above equations. As an example, consider the case where $\beta_\alpha(\mathbf{x})$ is uniform throughout the inclusion

$$\begin{aligned} p_\alpha(x,\xi) &= \delta(\xi-\bar{\beta}_\alpha), \quad p_\alpha(\xi_1,\xi_2;\boldsymbol{\tau},\boldsymbol{\upsilon}) \\ &= \delta(\xi_1-\bar{\beta}_\alpha)\delta(\xi_2-\bar{\beta}_\alpha), \end{aligned} \tag{55}$$

$$p_{LS}(\xi_1,\xi_2;\boldsymbol{\tau},\boldsymbol{\upsilon}) = \delta(\xi_1-\bar{\beta}_L)\delta(\xi_2-\bar{\beta}_S). \tag{56}$$

Making use of these in Eqs. (39)–(41), we have

$$\langle \beta_\alpha \rangle = \bar{\beta}_\alpha, \quad N_{\alpha\alpha}(\boldsymbol{\tau}, \boldsymbol{\upsilon}) = \bar{\beta}_\alpha^2, \quad N_{LS}(\boldsymbol{\tau}, \boldsymbol{\upsilon}) = \bar{\beta}_L \bar{\beta}_S. \tag{57}$$

It then follows from Eqs. (42)–(47) that

$$\langle A_j^L \rangle = \frac{iU^2 k_L^3}{2} [\bar{\beta}_L - (1 - \hat{x}_1^2)\bar{\beta}_S] \hat{x}_j V_L(\hat{\mathbf{x}}), \tag{58}$$

$$\langle A_j^S \rangle = \frac{iU^2 k_T^3}{2} (\delta_{j1} - \hat{x}_j \hat{x}_1) \hat{x}_1 \bar{\beta}_S V_S(\hat{\mathbf{x}}), \tag{59}$$

$$\langle A_j^L A_j^{L*} \rangle = \frac{U^4 k_L^6}{4} [\bar{\beta}_L - (1 - \hat{x}_1^2)\bar{\beta}_S]^2 V_L(\hat{\mathbf{x}}) V_L^*(\hat{\mathbf{x}}), \tag{60}$$

$$\langle A_j^S A_j^{S*} \rangle = \frac{U^4 k_T^6}{4} (1 - \hat{x}_1^2) \hat{x}_1^2 \bar{\beta}_S^2 V_S(\hat{\mathbf{x}}) V_S^*(\hat{\mathbf{x}}). \tag{61}$$

A practically more interesting, and more challenging, problem is to obtain the statistics of $\beta_\alpha(\mathbf{x})$ from the measured statistics of the scattered fields, i.e., to solve for $\langle \beta_\alpha \rangle$, $N_{\alpha\alpha}(\boldsymbol{\tau}, \boldsymbol{\upsilon})$, and $N_{LS}(\boldsymbol{\tau}, \boldsymbol{\upsilon})$ from the measured scattered fields $\mathbf{A}^\alpha$. This inverse problem in general does not have unique solutions. In what follows, we will attempt to solve this inverse problem for a simplified case.

We begin by assuming that $\beta_L(\mathbf{x})$ follows a Gaussian process, and the autocorrelation function is given by an exponential form

$$N(\boldsymbol{\tau}, \boldsymbol{\upsilon}) = \bar{\beta}_L^2 + \sigma^2 \exp(-\|\boldsymbol{\tau} - \boldsymbol{\upsilon}\|/\lambda), \tag{62}$$

where $\bar{\beta}_L$ is the mean, σ is the standard deviation, and λ is the autocorrelation length of $\beta_L(\mathbf{x})$. Further, we assume that experimental measurements have been obtained for the scattered fields, i.e., $A_j^\alpha(\hat{\mathbf{x}})$ have been measured experimentally. It then follows from Eqs. (51) and (53) that $\langle A_j^L \rangle_f$, $\langle A_j^L \rangle_b$, $\langle A_j^L A_j^{L*} \rangle_f$, and $\langle A_j^L A_j^{L*} \rangle_b$ can be computed from the experimentally measured $A_j^\alpha(\hat{\mathbf{x}})$. Our next task is to find $\bar{\beta}_L$, σ, and λ in terms of these measured quantities.

To this end, we first turn to Eq. (51). It is seen from the first part of Eq. (51) that $\bar{\beta}_L$ can be readily found once $\langle A_j^L \rangle_f$ is known. Next, substituting Eq. (62) into Eq. (52) and the second part of Eq. (54) yields

$$\langle \phi_L \phi_L^* \rangle_f = \bar{\beta}_L^2 V^2 + \sigma^2 \int_V \int_V \exp(-\|\boldsymbol{\tau} - \boldsymbol{\upsilon}\|/\lambda) d\boldsymbol{\tau} d\boldsymbol{\upsilon}, \tag{63}$$

$$\begin{aligned} \langle \phi_L \phi_L^* \rangle_b = {} & \bar{\beta}_L^2 \int_V \int_V \exp[4ik_L(\tau_1 - \upsilon_1)] d\boldsymbol{\tau} d\boldsymbol{\upsilon} \\ & + \sigma^2 \int_V \int_V \exp(-\|\boldsymbol{\tau} - \boldsymbol{\upsilon}\|/\lambda) \\ & \times \exp[4ik_L(\tau_1 - \upsilon_1)] d\boldsymbol{\tau} d\boldsymbol{\upsilon}. \end{aligned} \tag{64}$$

We note from Eqs. (51) and (53) that once the forward scattered and backscattered fields are measured experimentally, $\langle \phi_L \phi_L^* \rangle_f$ and $\langle \phi_L \phi_L^* \rangle_b$ are known. Therefore, Eqs. (63) and (64) provide a system of two equations from which the deviation σ and the correlation length λ can be obtained.

VI. EXAMPLE PROBLEM WITH SYNTHETIC DATA

To illustrate this procedure and its effectiveness, we consider an example where the inclusion is a sphere of radius R. To obtain the experimental data for $A_j^\alpha(\hat{\mathbf{x}})$, we first generate a set of $\{\beta_L(\mathbf{x})\}$ that follows the Gaussian distribution of

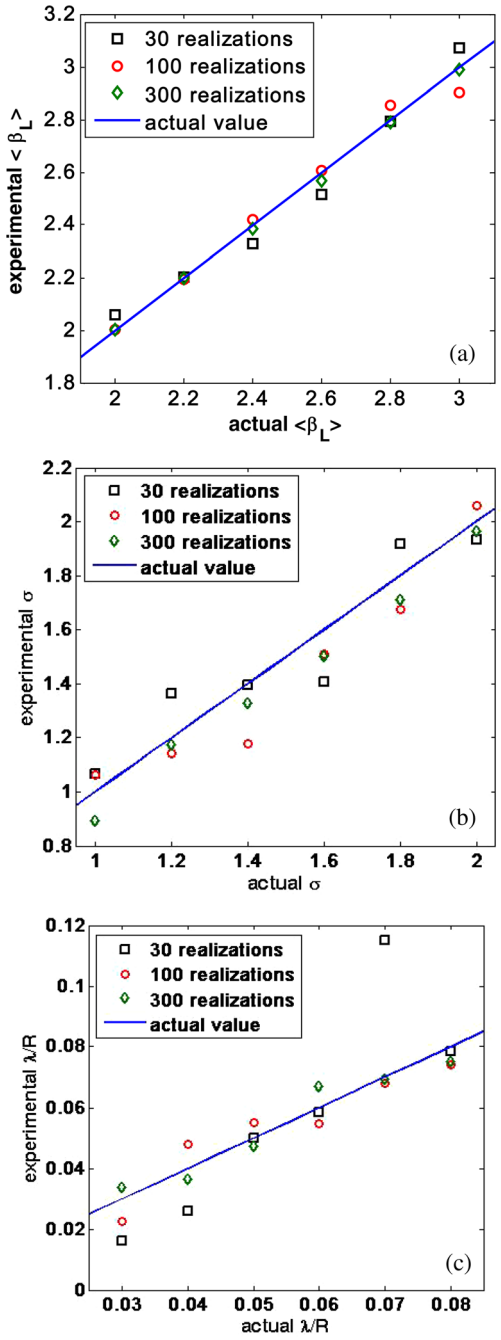

FIG. 3. (Color online) (a) Comparison between actual ensemble average of nonlinear parameter β_L to experimental (Monte Carlo simulation) ensemble average of nonlinear parameter β_L with different times of realization (three-dimension inclusion). (b) Comparison between actual standard deviation σ of nonlinear parameter β_L to experimental (Monte Carlo simulation) standard deviation σ of nonlinear parameter β_L with different times of realization (three-dimension inclusion). (c) Comparison between actual dimensionless autocorrelation length λ/R of nonlinear parameter β_L to experimental (Monte Carlo simulation) dimensionless autocorrelation length λ/R of nonlinear parameter β_L with different times of realization (three-dimension inclusion).

which the autocorrelation function is given by Eq. (62) with given values of $\bar{\beta}_L$, σ, and λ. These given statistical parameters are called the actual values. For each $\beta_L(\mathbf{x})$, the forward scattered field $A_j^{\alpha}(\hat{\mathbf{x}}^f)$ and backscattered field $A_j^{\alpha}(\hat{\mathbf{x}}^b)$ will be computed from Eqs. (35) and (37), respectively. Thus, one can generate a set of $\{A_j^{\alpha}(\hat{\mathbf{x}}^f)\}$ and $\{A_j^{\alpha}(\hat{\mathbf{x}}^b)\}$. We will regard this set of synthetic forward scattered and backscattered data as the "experimental" data. The quality of these synthetic experimental data depends on the number of realizations used to generate $\{\beta_L(\mathbf{x})\}$. The more realizations used, the closer are $A_j^{\alpha}(\hat{\mathbf{x}}^f)$ and $A_j^{\alpha}(\hat{\mathbf{x}}^b)$ to their expected values.

Next, we will use these synthetic experimental data to compute $\langle A_j^L\rangle_f$, $\langle A_j^L\rangle_b$, $\langle A_j^L A_j^{L*}\rangle_f$, and $\langle A_j^L A_j^{L*}\rangle_b$. These computed values are then used in Eqs. (51), (53), and (63) and (64) to obtain $\bar{\beta}_L$, σ, and λ. The $\bar{\beta}_L$, σ, and λ so obtained will be regarded as the experimental results. Figures 3(a)–3(c) show the comparison between the experimental results and actual values of $\bar{\beta}_L$, σ, and λ. In Figs. 3(a)–3(c), we have six groups of $\{\beta_L(\mathbf{x})\}$ with different $\bar{\beta}_L$, σ, and λ. The horizontal axis stands for different actual values of $\bar{\beta}_L$, σ, and λ/R, while the vertical axis shows the corresponding experimental values. It is seen that results based on about 300 or more realizations are very accurate.

Before closing, we note that the above method assumes that the distribution of $\beta_L(x)$ is Gaussian. A much more challenging problem is how to find what the distribution medium is.

VII. SUMMARY AND CONCLUSIONS

This paper investigates the scattering of a time-harmonic plane wave by an elastic inclusion with heterogeneous quadratic nonlinearity. Both the near and far fields of the scattered second harmonic waves are obtained in terms of the Green's function of the matrix material. Major findings of this investigation include: (1) the scattered second harmonic fields depend on the nonlinear properties of the inclusion through two independent acoustic nonlinearity parameters, β_L and β_S, both of which are functions of the second and third order elastic constants; (2) under longitudinal wave incidence, the scattered wave fields contain both longitudinal and shear second harmonic waves, and the second harmonic shear wave disappears when $\beta_S = 0$; (3) in the near field, a "static" displacement corresponding to the radiation induced eigenstrain (Qu *et al.*, 2011) is present. This static displacement vanishes in the far field.

Also considered in this study is the case when the nonlinear properties of the inclusion are given as random functions. The statistics of the scattered second harmonic waves, such as the ensemble average, deviation, autocorrelation, and cross-correlation, are obtained in terms of the corresponding statistics of the acoustic nonlinear parameters of the inclusion. Furthermore, a methodology is developed to solve the inverse problem, i.e., obtaining the statistics of the acoustic nonlinearity parameters from scattered second harmonic waves. It is shown that by experimentally measuring the forward and backscattered second harmonic waves, one can nondestructively estimate the statistics of the acoustic nonlinearity parameters of the inclusion.

ACKNOWLEDGMENTS

The research was supported in part by the National Science Foundation (CMMI-0653883), by the Air Force Office of Scientific Research (FA9550-08-1-0241), and by the Infrastructure Technology Institute at Northwestern University.

Achenbach, J. D., Gautesen, A. K., and McMaken, H. (**1982**). "Wave motions generated by a point load," in *Ray Methods for Waves in Elastic Solids—With applications to scattering by cracks* (Pitman Advanced Publishing Program, Boston/London/Melbourne), pp. 22–27.

Bermes, C., Kim, J. Y., Qu, J. M., and Jacobs, L. J. (**2007**). "Experimental characterization of material nonlinearity using Lamb waves," Appl. Phys. Lett. **90**, 021901.

Bermes, C., Kim, J. Y., Qu, J. M., and Jacobs, L. J. (**2008**). "Nonlinear Lamb waves for the detection of material nonlinearity," Mech. Syst. Signal Process. **22**, 638–646.

Breazeale, M. A., and Thompson, D. O. (**1963**). "Finite-amplitude ultrasonic waves in aluminum," Appl. Phys. Lett. **3**, 77–78.

Cantrell, J. H. (**2004a**). "Fundamentals and applications of nonlinear ultrasonic nondestructive evaluation," in *Ultrasonic NDE for Engineering and Biological Material Characterization*, edited by T. Kundu (CRC Press, Boca Raton), pp. 311–362.

Cantrell, J. H. (**2004b**). "Substructural organization, dislocation plasticity and harmonic generation in cyclically stressed wavy slip metals," Proc. R. Soc. London, Ser. A **460**, 757–780.

Cantrell, J. H., Jr. (**1984**). "Acoustic-radiation stress in solids. I. Theory," Phys. Rev. B (Condensed Matter) **30**, 3214–3220.

Cantrell, J. H., Yost, W. T., and Li, P. (**1987**). "Acoustic radiation-induced static strains in solids," Phys. Rev. B (Condensed Matter) **35**, 9780–9782.

Donskoi, D. M., and Sutin, A. M. (**1980**). "Sound scattering due to nonlinearity of the medium," Sov. Phys. Acoust. **26**, 224–226.

Donskoi, D. M., and Sutin, A. M. (**1984**). "Nonlinear scattering and propagation of longitudinal acoustic-waves in porous-media," Sov. Phys. Acoust. **30**, 358–361.

Herrmann, J., Kim, J. Y., Jacobs, L. J., Qu, J. M., Littles, J. W., and Savage, M. F. (**2006**). "Assessment of material damage in a nickel-base superalloy using nonlinear Rayleigh surface waves," J. Appl. Phys. **99**, 124913.

Hikata, A., Chick, B. B., and Elbaum, C. (**1965**). "Dislocation contribution to the second harmonic generation of ultrasonic waves," J. Appl. Phys. **36**, 229–236.

Hikata, A., and Elbaum, C. (**1966**). "Generation of ultrasonic second and third harmonics due to dislocations I," Phys. Rev. **144**, 469–477.

Jones, G. L., and Korbett, D. R. (**1963**). "Interaction of elastic waves in an isotropic solid," J. Acoust. Soc. Am. **35**, 5–10.

Keck, W., and Beyer, R. T. (**1960**). "Frequency spectrum of finite amplitude ultrasonic waves in liquids," Phys. Fluids **3**, 346–352.

Kim, J. Y., Jacobs, L. J., Qu, J., and Littles, J. W. (**2006a**). "Experimental characterization of fatigue damage in a nickel-base superalloy using nonlinear ultrasonic waves," J. Acoust. Soc. Am. **120**, 1266–1273.

Kim, J. Y., Qu, J., Jacobs, L. J., Littles, J. W., and Savage, M. F. (**2006b**). "Acoustic nonlinearity parameter due to microplasticity," J. Nondestruct. Eval. **25**, 28–36.

Lamb, H. (**1925**). *Dynamical Theory of Sound* (Edward Arnold and Company, London), pp. 177–185.

Nazarov, V. E., Ostrovsky, L. A., Soustova, I. A., and Sutin, A. M. (**1988**). "Nonlinear acoustics of micro-inhomogeneous media," Phys. Earth Planet. Inter. **50**, 65–73.

Norris, A. N. (**1997**). "Finite-amplitude waves in solids," in *Nonlinear Acoustics*, edited by M. F. Hamilton and D. T. Blackstock (Academic Press, San Diego), pp. 263–277.

Ostrovsky, L. A., Sutin, A. M., Soustova, I. A., Matveyev, A. L., Potapov, A. I., and Kluzek, Z. (**2003**). "Nonlinear scattering of acoustic waves by natural and artificially generated subsurface bubble layers in sea," J. Acoust. Soc. Am. **113**, 741–749.

Pruell, C., Kim, J. Y., Qu, J., and Jacobs, L. J. (**2007**). "Evaluation of plasticity driven material damage using Lamb waves," Appl. Phys. Lett. **91**, 231911.

Qu, J., and Cherkaoui, M. (**2006**). *Fundamentals of Micromechanics of Solids* (John Wiley & Sons, Inc., Hoboken, NJ), pp. 71–72.
Qu, J., Jacobs, L. J., and Nagy, P. B. (**2011**). "On the acoustic-radiation-induced strain and stress in elastic solids with quadratic nonlinearity," J. Acoust. Soc. Am. **129**, 3349–3452.
Smith, R. T., Stern, R., and Stephens, R. W. (**1966**). "Third-order elastic moduli of polycrystalline metals from ultrasonic velocity measurements," J. Acoust. Soc. Am. **40**, 1002–1008.
Sokolov, A. Y., and Sutin, A. M. (**1983**). "Scattering of the 2nd harmonic of an acoustic-wave in a liquid containing gas-bubbles," Sov. Phys. Acoust. **29**, 59–61.
Suzuki, T., Hikata, A., and Elbaum, C. (**1964**). "Anharmonicity due to glide motion of dislocations," J. Appl. Phys. **35**, 2761–2766.
Thompson, R. B., Buck, O., and Thompson, D. O. (**1976**). "Higher harmonics of finite-amplitude ultrasonic-waves in solids," J. Acoust. Soc. Am. **59**, 1087–1094.
Thompson, R. B., and Tiersten, H. F. (**1977**). "Harmonic-generation of longitudinal elastic-waves," J. Acoust. Soc. Am. **62**, 33–37.
Thurston, R. N., and Shapiro, M. J. (**1967**). "Interpretation of ultrasonic experiments on finite-amplitude waves," J. Acoust. Soc. Am. **41**, 1112–1125.
Zhou, S., and Shui, Y. (**1992**). "Nonlinear reflection of bulk acoustic-waves at an interface," J. Appl. Phys. **72**, 5070–5080.
Zverev, V. A., and Kalachev, A. I. (**1968**). "Measurement of scattering of sound by sound in superposition of parallel beams," Sov. Phys. Acoust. **14**, 173–178.